

## Dynamic Behavior Caused by Bifurcation Property of Radial Electric Field in a Toroidal Helical Plasma of CHS

FUJISAWA Akihide\*, IGUCHI Harukazu, MINAMI Takashi, YOSHIMURA Yasuo, TANAKA Kenji, ITOH Kimitaka, SANUKI Heiji, KOJIMA Mamoru, ITOH Sanae-I.<sup>1</sup>, YOKOYAMA Masayuki, OKAMURA Shoichi, IDA Katsumi, ISOBE Mitsutaka, NISHIMURA Shin, OSAKABE Masaki, NOMURA Izumi, SHIMIZU Akihiro, TAKAHASHI Chihiro, MATSUOKA Keisuke, HAMADA Yasuji and FUJIWARA Masami

National Institute for Fusion Science, Toki, Japan, 509-5292

<sup>1</sup>RIAM, Kyushu University, Kasuga 816-8580 Japan

(Received: 5 December 2000 / Accepted: 17 August 2001)

### Abstract

Bifurcation properties in radial electric field have been studied using a heavy ion beam probe in a toroidal helical plasma of Compact Helical System. This paper presents an overview of the bifurcation phenomena observed in potential structure and its dynamics, such as potential patterns with transport barrier formation, and self-organized oscillation termed *electric pulsation*. Detailed analysis of this oscillatory state provides an interesting result of spatio-temporal evolutions of potential and density profile during a pulse-like event.

### Keywords:

radial electric field, bifurcation and transition, electric pulsation, internal transport barrier, CHS, HIBP, neoclassical theory, pattern formation,  $E_r$ -shear

### 1. Introduction

Plasma is a non-equilibrium matter with rich nonlinearity, where bifurcation phenomena may be expected. In fact, the discovery of the H-mode in the ASDEX tokamak [1] proves the bifurcation nature of toroidal plasmas. There, the bifurcation in transport property results in a sudden change of its structure. Also nonlinear oscillations, edge localized modes (ELMs), have been observed and considered to be repetitive transitions between two distinct structures, L- and H-modes. Many theories and experiments show that these phenomena should be ascribed to the bifurcation of the radial electric field ( $E_r$ ) [2-6].

The bifurcation nature of toroidal helical plasmas has been expected with neoclassical theories including helical ripple effects on the transport [7,8]. In such

theories, radial electric field is highly nonlinear, especially in a low collisional regime, and solitary wave solutions were found in evolution of radial electric field [9]. Actually, a number of bifurcation phenomena have been observed in the experiments of a toroidal helical plasma in Compact Helical System (CHS) [10].

This paper describes patterns of potential profiles observed in electron cyclotron resonance (ECR) heated plasmas. The appearance of the patterns is expressed in a bifurcation diagram on a plane of central potential and density. A dynamic bifurcated state of nonlinear oscillation is introduced with its analysis of spatio-temporal evolutions of potential and density profiles. The experimental bifurcation property is discussed in association with the neoclassical property.

\*Corresponding author's e-mail: fujisawa@nifs.ac.jp

## 2. Experimental Devices

In the Compact Helical System (CHS) [11], the structure of internal electrostatic potential has been investigated using a heavy ion beam probe (HIBP). The CHS is a heliotron/torsatron device whose major and minor radii are 1.0 m and 0.2 m, respectively. The aspect ratio of approximately 5 is the lowest in toroidal helical devices at present. The helical ripple coefficient at the edge is  $\epsilon_H \sim 0.3$ , that is comparable to the inverse aspect ratio of about 0.2.

The CHS device is equipped with an HIBP whose beam energy is up to 200 keV. The HIBP has, in principle, the capability in simultaneous measurements of potential, density, magnetic field and their fluctuation [12]. In this HIBP, an additional beam sweep system is set in front of the energy analyzer as well as on the accelerator side. By using two sweep systems, the complicated beam trajectory in the magnetic field of a toroidal helical device is managed to extend the observable range widely over almost the whole plasma region [13].

Cesium beam of 72 keV is used for the configuration where the presented experiments are performed. In the HIBP measurements, potential profile is obtained by sweeping the beam trajectory continuously. Time evolution of potential can be obtained in every a few millisecond at the fastest. On the other hand, dynamics or fluctuation of plasma can be detected when the beam orbit, or observation point, is fixed. A high temporal resolution up to approximately 500 kHz is attainable by tuning the gain of current-voltage converters.

## 3. Bifurcation Characteristics

### 3.1 Stationary Bifurcated Branches

In the CHS plasmas, the observed potential has been classified into five identical patterns. Figure 1a shows the typical potential profiles for these five patterns. The patterns are termed *bell*, *dome*, *hill*, *Mexican-hat* and *well* in order from the higher to the lower central potential value.

The Neutral Beam Injection (NBI)-heated plasmas only show well-pattern, while the electron cyclotron resonance (ECR) heated plasmas do every patterns according to the line-averaged density and the ECR-heating power. As collisionarity becomes lower by increasing the heating power or decreasing the line-averaged density, the central potential becomes higher. In other words, positive potential patterns of hill, dome and bell turn to be more probable. These three are considered as bifurcated patterns in a low density

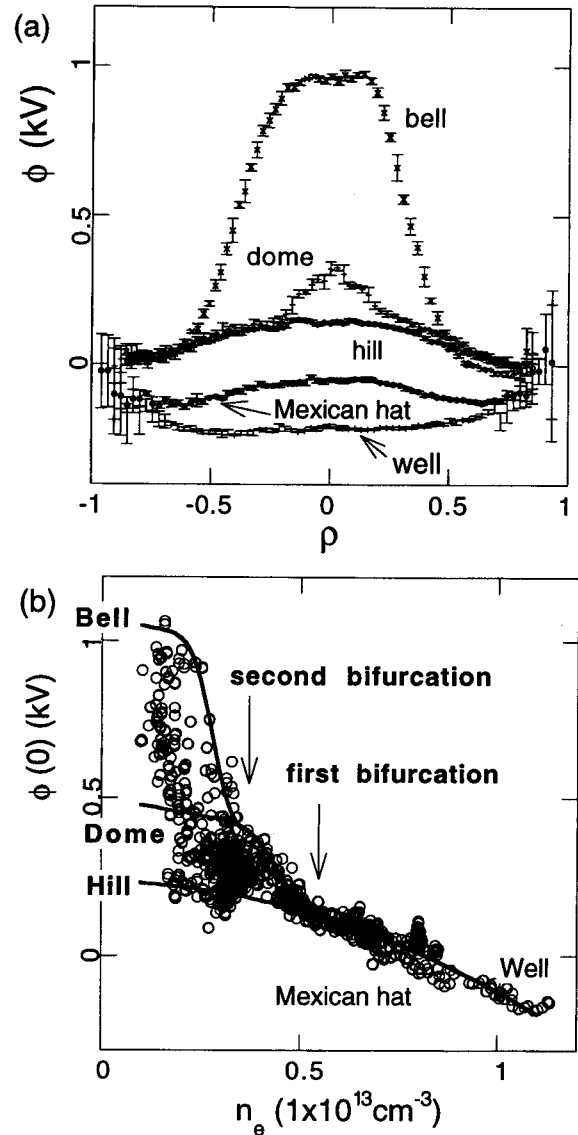


Fig. 1 (a) Representative shapes of potential profiles that have been ever observed in CHS. (b) Dependence of the central potential on the line-averaged density in the case of ECR heating power of 100 kW. In low density regimes, bifurcations of the potential profile are observed at two critical values of density. Characteristic shapes of potential profiles are identical for five regimes.

regime, since transitions between bell, dome and hill patterns (or discrete changes in patterns) have been observed [14,15]. On the other hand, the hill, Mexican-hat and well profiles can change continuously as the line-averaged density alters.

Figure 1b shows dependence of the pattern on the line-averaged density. In the diagram, the change of the

pattern is expressed in terms of the central potential values for ECR-heated plasmas, where its heating power is fixed at approximately 100 kW. The central potential decreases with an increase in the line-averaged density along three bifurcated branches; hill, dome and bell branches. The diagram indicates two critical values of density where bifurcation in potential profile pattern occurs. At the first critical density of  $\bar{n}_e \approx 0.5 \times 10^{13} \text{ cm}^{-3}$ , the potential pattern bifurcates into hill and dome branches. As density decreases further and reaches the second critical value of  $\bar{n}_e \approx 0.3 \times 10^{13} \text{ cm}^{-3}$ , the potential pattern bifurcates into dome and bell-branches. The change from dome to bell pattern can be characterized by outward movement of the maximum  $E_r$ -shear radius from  $\rho \approx 0.3$  to  $\rho \approx 0.5$ . In this low ECR-heating power ( $P_{\text{ECRH}} \approx 100 \text{ kW}$ ), the realization of the hill branch is most probable amongst the three bifurcated branches in that low density region [15].

### 3.2 Oscillatory States - Emergence of Electric Pulsation

As the ECR-heating power increases, branches of dome and bell become more probable to be realized than the hill branch. Furthermore, an increase in the ECR-heating power realizes a dynamic oscillatory state, that is termed *electric pulsation* [16]. The most dynamic example is shown in Fig. 2. This examples are from hydrogen plasmas to which almost maximum ECR-

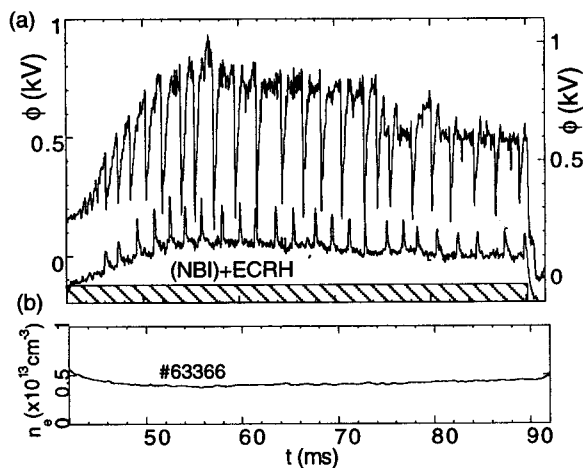


Fig. 2 (a) Pulsating behavior of the potentials at the center and at an outer radius of  $\rho = 0.59$  in the CHS plasmas. This phenomenon is referred to as electric pulsation. The example is observed in a combined ECH + NBI heating phase. (b) The time evolution of the line averaged electron density measured with an HCN interferometer.

heating power ( $P_{\text{ECRH}} \approx 300 \text{ kW}$ ) is applied to the NBI-sustained plasma. The solid lines in Fig. 2 show waveforms of central potential and at an outer radius of  $\rho = 0.59$  in the CHS plasmas.

In this discharge, the self-organized oscillation is maintained for a period ( $t \approx 50 \sim 90 \text{ ms}$ ) in a combined phase of the ECR and NBI heating. In that period, the waveform at the center exhibits negative pulses with its amplitude of  $-0.6 \text{ kV}$  quasi-periodically, while that at  $\rho = 0.59$  shows quasi-periodic positive pulses with the same interval. In both waveforms the pulse-like event occurs in approximately every 2 ms, or with frequency of  $\sim 0.5 \text{ kHz}$ . The timescale of a pulse ( $\sim$  a few dozen microseconds) is much faster than the diffusive one ( $\sim$  a few milliseconds). The oscillation can be recognized as repetitive transitions between quasi-equilibrium states (see the next section), although the life time of the lower potential state is much shorter than that of higher potential state. The other plasma parameters are also pulsating being synchronized with the potential pulses.

At the same ECR-heating power as the case of Fig. 2, the amplitude and frequency alter with the line-averaged density. The pulsation frequency increases and the pulse amplitude decreases, with an increase in the density. By changing the ECR-heating power, we have observed a number of variation of pulsation patterns [10]. At the power threshold, the repetitive transitions are observed to occur between two branches, for example, dome and hill. There the life time of hill and dome are almost similar [15].

### 4. Transport Barrier Formation

In the five patterns of profile profiles, the dome and bell-profiles have a rather large  $E_r$ -shear at radii of  $\rho \approx 0.3$  and  $\rho \approx 0.5$ , respectively. According to the present paradigm of  $E_r$ -shear reduction of fluctuation, transport barrier formation is expected at those radii. In fact, electron thermal transport barrier has been confirmed for plasmas with the dome pattern profile [17].

Figure 3a shows  $E_r$ -structure around the transport barrier, using  $\tanh[r/\alpha]$ -function. The position of the maximum  $E_r$ -shear is located at the normalized radius of  $\rho \approx 0.3$ . The maximum value is estimated as approximately  $40 \text{ V/cm}^2$ , and the full width of half maximum of  $E_r$ -shear is approximately 1.4 cm. Figure 3b illustrates the density fluctuation power; in that low density regime of  $\bar{n}_e \approx 0.5 \times 10^{13} \text{ cm}^{-3}$ , the fluctuation in the detected beam current  $\delta I_b(r)$  well reflects local fluctuation of density at the ionization point [18]. The fluctuation reduction is reduced by 48 % at  $E_r$ -shear

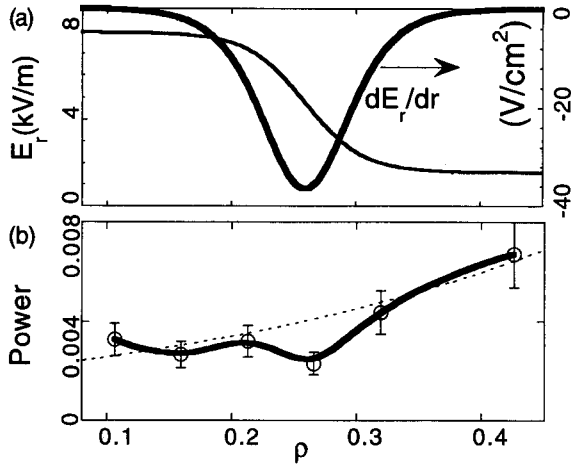


Fig. 3 (a) Fine structure of radial electric field and its shear around the transport barrier. (b) Density fluctuation ( $\delta n_e/n_e$ ) integrated from 5 kHz to 70 kHz around the barrier measured with the HIBP. Here, circles represents the fluctuation for the dome state with the transport barrier. The fluctuation (in arbitrary unit) in the hill state is shown by the dashed line as a reference.

maximum radius. The result supports the present paradigm that  $E_r$ -shear should reduce the fluctuation, and should contribute to the formation of transport barrier. In case of the plasmas with bell-feature, the maximum  $E_r$ -shear is found approximately 60 V/cm<sup>2</sup> at the radial position of  $\rho \approx 0.5$ , therefore, the fluctuation reduction and formation of transport barrier are expected. The similar feature of electron temperature profile has been recently observed in Wendelstein 7-AS and TJ-II stellarators [19,20].

## 5. Barrier Front Dynamics

### 5.1 Reconstruction of Potential Profile Evolution During Pulsation

A detailed analysis of the previous example of electric pulsation indicates that the electric pulsation is not simply recognized as repetitive transitions between two distinct states. The good correlation between soft x-ray signal and potential pulse allows to reconstruct the spatio-temporal evolution of potential profile during pulsation by taking the central chord of soft x-ray signal as a reference clock. In a discharge, more than a dozen pulses are available to produce their statistically averaged waveforms of potential.

Figure 4a shows the evolution of the reconstructed potential profiles during transitions, using these time-averaged waveforms. Closed circles represent the profile

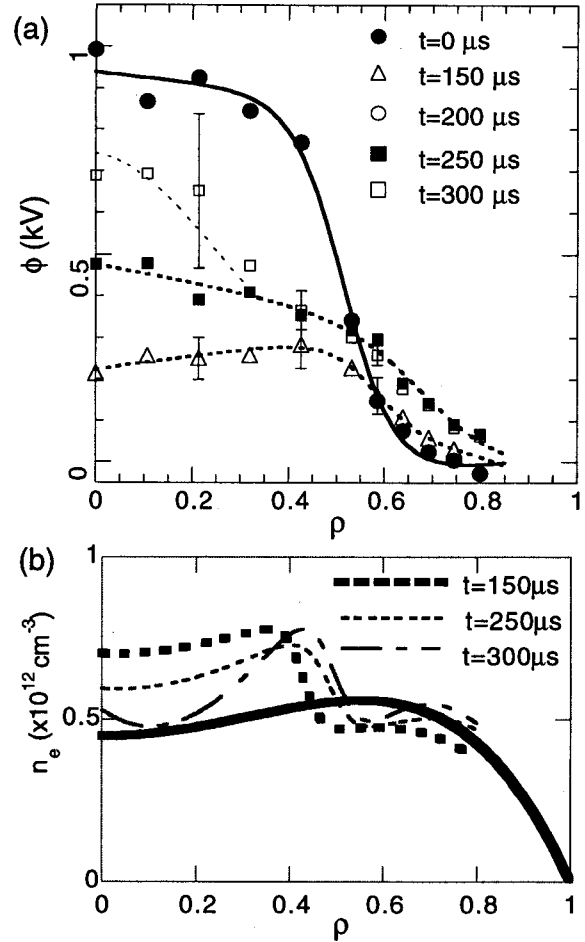


Fig. 4 (a) Evolution of reconstructed potential profile during electric pulsation. The potential profile in the high potential state at  $t = 0 \mu\text{s}$  is represented by the closed circles. The potential profiles after the transition are shown at  $t = 150 \mu\text{s}$ ,  $t = 250 \mu\text{s}$  and  $t = 300 \mu\text{s}$ . (b) Evolution of reconstructed density profile during electric pulsation using the detected beam current signals. The bold line indicates the density profile with Abel-inversion in the high potential state. This suggests the density profile after transition from the high to the low potential state becomes a centrally-peaked one.

at the high potential state ( $t = 0 \mu\text{s}$ ), that is the initial potential profile with the bell feature. The first transition happens in radial electric field around  $\rho \approx 0.5$ , and the potential profile changes into a shape represented by the open circles at  $t = 150 \mu\text{s}$ . During the next hundred microseconds until  $t = 250 \mu\text{s}$ , the radial electric field at the periphery becomes positive, and the potential profile alters its shape a little slowly. After the plasma shows the profile indicated by the closed squares ( $t \approx 250 \mu\text{s}$ ),

another transition occurs around the core at  $\rho \approx 0.3$ . Then the plasma takes the intermediate potential profile with the dome feature, represented by the open squares, at  $t \approx 300 \mu\text{s}$ . The potential profile rather gradually recovers to the initial state. In other words, the foot point of a strong shear of the radial electric field moves outwards. In approximately 2 ms later, almost the same process is repeated.

The detected beam current also exhibits a good correlation with the soft X-ray signals and the potential signal in a wide range of minor radius. The density of the discharges is sufficiently low for us to ascribe the change in the detected beam current to a local density change. This allows to deduce a transient change of density profile during the pulsation except the plasma edge [18]. The density profile can be reconstructed using the time-averaged values of interferometer signals including pulses. The density profile obtained in this process should mainly reflect high potential state owing to its longer life time, although some small contribution in the low potential state is involved.

Similarly to the previous treatment of potential signals, statistical averages of the beam current signals during a pulse are obtained by taking the central chord of soft X-ray as a reference clock. Assuming that the path integral effect is completely neglected, the ratio of beam current before and after transitions  $I_B(t)/I_B(t=0)$  are supposed to purely reflect the ratio of the local density change  $n_e(t)/n_e(t=0)$ . Hence, evolution of the density profile during the pulsation can be inferred by multiplying the ratio to the Abel inverted density profile in the high potential state.

Figure 4b shows evolution of the reconstructed density profiles. The ratios and the reconstructed density profiles are presented at three points of time,  $t = 150 \mu\text{s}$ ,  $t = 250 \mu\text{s}$  and  $t = 300 \mu\text{s}$ . At the time of  $t = 150 \mu\text{s}$ , a clear boundary of the change is seen at the location of  $\rho \sim 0.4$ . The density increases inside the boundary, while it decreases outside. Then, the density profile recovers to the initial values of the high potential state after the density profile modification becomes to be localized around the boundary.

The increase in density from  $t = 0 \mu\text{s}$  to  $t = 150 \mu\text{s}$  is from  $\bar{n}_e(0) \approx 0.4 \times 10^{13} \text{ cm}^{-3}$  to  $\bar{n}_e(0) \approx 0.7 \times 10^{13} \text{ cm}^{-3}$ . The amount of change is quite large. In order to explain this increase in density, necessary change of particle fluxes is approximately  $\delta\Gamma \sim 3 \times 10^{16} \text{ cm}^{-2} \text{ s}^{-1}$  at  $\rho \sim 0.4$ . The neoclassical fluxes accompanied with the absolute value of radial electric field, however, is predicted to be only about  $\delta\Gamma \sim 10^{15} \text{ cm}^{-2} \text{ s}^{-1}$ . Another mechanism

should, therefore, play a role in the reformation of density profile. A possible candidate is convective fluxes induced by poloidal asymmetry in potential during the pulsation. The detailed analysis clearly demonstrates that more interesting detail exists to be investigated in the electric pulsation.

## 6. Neoclassical Property of Radial Electric Field

The bifurcation nature of radial electric field, that should be related with the phenomena introduced in this paper, has been predicted by the neoclassical theory. Here, we briefly present an example of the neoclassical bifurcation characteristics as follows.

A neoclassical calculation for hydrogen is shown in Fig. 5. Here, we use the Hastings formula to solve the ambipolar condition  $\Gamma_i^{na}(E_r) = \Gamma_e^{na}(E_r)$  [7,8], the assumed parameters are shown in the Figure caption. We choose  $\epsilon_h = 0.063$  and  $\epsilon_t = 0.16$ , where  $\epsilon_h$  and  $\epsilon_t$  are helical ripple coefficient and toroidal coefficient (or inverse aspect ratio), respectively. Figure 5a show equi-contours of  $E_r$  on the  $n_e$ - $T_e$  plane, and the painted crescent region indicates an area where two stable and an unstable roots exist. The contour of  $E_r = 0$  is indicated by the bold dashed line. The other contours of constant electric field are also shown by the thin dashed lines.

Figures 5b and 5c present changes of radial electric field along lines crossing the crescent region. Both curves have a bifurcation nature of the radial electric field. However, as is shown in Fig. 5a, the electric field is uniquely defined above  $n_e \sim 1.5 \times 10^{13} \text{ cm}^{-3}$ . No bifurcation phenomenon, hence, is expected above the critical density. This feature should be associated with the experimental observation that the bifurcation phenomena have not been observed in a higher density regime at a fixed ECR-heating power.

The ripple coefficients of this example correspond to  $\rho \approx 0.5$  of the CHS plasma. Similar diagrams of neoclassical bifurcation can be drawn for other radial positions of CHS. The experimental results obtained to date have not shown any contradiction to neoclassical expectation in terms of transition time scale, and plasma parameters where the bifurcation phenomena occur, within the present precision.

## 7. Discussion and Conclusion

The spatio-temporal patterns of potential introduced here can be interpreted on the basis of the neoclassical bifurcation property. A neoclassical calculation can produce the patterns observed in the experiments [21].

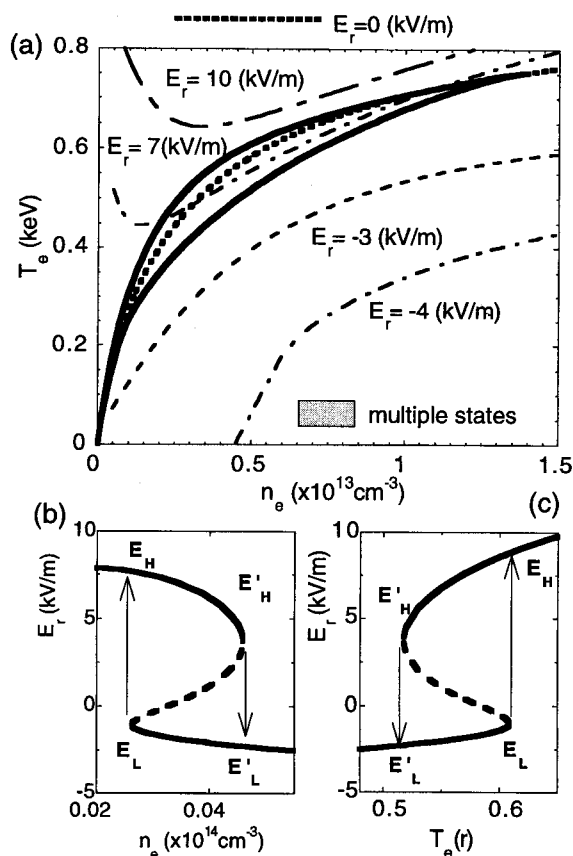


Fig. 5 An example of neoclassical calculation. The assumptions used in the calculation are  $T_i(\rho) = 300$  eV,  $Z_{\text{eff}} = 2$ ,  $\partial \ln n_e(\rho) / \partial \rho = 0$  and  $\partial \ln T_e(\rho) / \partial \rho = \partial \ln T_i(\rho) / \partial \rho = -1.1$ . We choose  $\varepsilon_n = 0.063$  and  $\varepsilon_t = 0.16$ , which corresponds to  $\rho \approx 0.5$  of the CHS hydrogen plasma. (a) Region where multiple steady states exist in  $n_e$ - $T_e$  plane (painted region). Contours of constant electric field are shown by dashed lines. (b) Bifurcation curve of radial electric field as a function of density.  $T_e(\rho) = 0.5$  keV is assumed. (c) Bifurcation curve of radial electric field as a function of temperature.  $n_e(\rho) = 5 \times 10^{12} \text{ cm}^{-3}$  is assumed.

In potential profile of dome (or bell), the radial electric field inside  $\rho \approx 0.3$  (or  $\rho \approx 0.5$ ) belongs to higher field branch, while the outside field still remains in low field branch. In the connection layer at which two bifurcated  $E_r$ -branches converge, rather strong  $E_r$ -shear is created to form the transport barrier. Better transport property of positive  $E_r$  should partially contribute to improving the confinement in the core region.

The  $E_r$ -structure around the barrier allows us to estimate the momentum diffusivity, or the viscous coefficient, using the diffusion equation for radial electric field;  $\mu \varepsilon_0 \varepsilon_{\perp} \partial^2 E_r / \partial r^2 + j_r(E_r) = 0$ , where  $\mu$  and

$\varepsilon_0 \varepsilon_{\perp}$  represent the viscous coefficient and the dielectric constant of the plasma, respectively [22]. Assuming that  $j_r$  is a cubic function of  $E_r$  (corresponding to the neoclassical expectation), the above diffusion equation gives a solution whose function form is  $\tanh[r/\Delta]$  with  $\Delta \propto \sqrt{\mu \varepsilon_0 \varepsilon_{\perp} \Delta E / \Delta j_r^M}$ , where  $\Delta E_r$  is the difference between the radial electric fields inside and outside the barrier, respectively, and  $\Delta j_r^M$  corresponds to the difference between the maximum radial currents during the back and forth transitions between the radial electric fields. The difference of the radial current is experimentally deduced as  $\Delta j_r^M \sim 5 \text{ A/m}^2$  [23]. The difference of radial electric field  $\Delta E_r$  is  $\sim 6$  kV/m. The dielectric constant  $\varepsilon_0 \varepsilon_{\perp}$  is estimated as  $1.3 \times 10^{-8} \text{ F/m}$ . Then, the viscous coefficient  $\mu$  is  $\sim 5 \text{ m}^2/\text{s}$ , which is comparable to the electron thermal diffusivity. The *anomalous* viscous coefficient can be affected by  $E_r$ -structure, as is similar to the thermal diffusivity. Consequently, the  $E_r$ -structure around the barrier may have a mutual link, that results in a more complicated  $E_r$ -structure than the simple form of  $\tanh[r/\Delta]$ . Finer structural measurements around the barrier are an interesting future work.

During the electric pulsation, the change of the radial electric field can be regarded as a limit cycle in the bifurcation curves, if the electric pulsation is observed at a radius; for example,  $\rho \approx 0.3$ , the foot-point of the barrier for dome-profile. However, the detailed analysis of the electric pulsation in Fig. 2 shows that the reality should be more complicated. It indicates that during the pulse the potential profile changes rather slowly from dome to the bell pattern. Several processes can be deduced during the pulse-like event; first, transition from bell to hill-like profile, second, transition from hill to dome-profile, finally the profile changes from dome to bell profile rather gradually.

An asymmetrical change in potential is suggested to explain the rapid change in density profile during the pulsation. There non-local effect may play an important role on the structural reformation. A number of experimental observations exist to show that an event happening at a point propagates to other points more rapidly than in diffusive time scales [24,25]. This is a quite unique feature with the structural formation in plasmas, compared to many other examples of dissipative structures, or self-organized systems. In order to pursue this non-local effect in plasmas, it is essential to measure physics quantities at different radii using diagnostics with high spatio-temporal resolution. This is an important future work.

In conclusion, we have presented several examples

of bifurcation phenomena observed in toroidal helical plasmas produced in CHS. In plasmas, thermal variables such as temperature and density are nonlinearly coupled with electric and magnetic fields, and its structure is self-consistently determined by mutual links between these variables; for instance,  $E_r$ -structure changes transport, then transport changes thermal variables (temperature, density and so on), finally temperature and density determine radial electric field again. The structure of the plasma cannot be determined not only by local property but also by long range interaction (non-local effect). As is shown in the present experiments of CHS, the plasmas provides us, therefore, an newly interesting object to be investigated as a nonlinear and non-equilibrium system [26].

### References

- [1] F. Wagner *et al.*, Phys. Rev. Lett. **49**, 1408 (1982).
- [2] For review, K. Itoh and S.-I. Itoh, Phys. Control. Fusion **38**, 1 (1996)
- [3] S.-I. Itoh and K. Itoh, Phys. Rev. Lett. **60**, 2276 (1988).
- [4] K.C. Shaing and E. Crume, Jr., Phys. Rev. Lett. **63**, 2369 (1989).
- [5] R.J. Groebner, K.H. Burrell, H. Niedermayer *et al.*, Phys. Rev. Lett. **64**, 3015 (1990).
- [6] K. Ida, S. Hidekuma, Y. Miura *et al.*, Phys. Rev. Lett. **65**, 1364 (1990).
- [7] D.E. Hastings, W.A. Houlberg and K.C. Shaing, Nucl. Fusion **2**, 445 (1985).
- [8] L.M. Kovrizhnykh, Nucl. Fusion **24**, 435 (1984).
- [9] D.E. Hastings, R.D. Hazeltine and P.J. Morrison, Phys. Fluid **29**, 69 (1986).
- [10] A. Fujisawa, H. Iguchi, T. Minami *et al.*, Phys. Plasma **7**, 4152 (2000).
- [11] K. Matsuoka, S. Kubo, M. Hosokawa *et al.*, in Plasma Physics and Controlled Nuclear Fusion Research 1988 (*Proc. 12th Int. Conf. Nice, 1988*), International Atomic Energy Agency, Vienna, 1989, Vol. 2, 411.
- [12] T.P. Crowley, IEEE Trans. on Plasma Phys. Sci. **22**, 291 (1994).
- [13] A. Fujisawa, H. Iguchi, S. Lee, T.P. Crowley, Y. Hamada, S. Hidekuma and K. Kojima, Rev. Sci. Instrum. **67**, 3099 (1996).
- [14] A. Fujisawa, H. Iguchi, T. Minami *et al.*, J. of Plasma and Fusion Res. **75**, 604 (1999).
- [15] A. Fujisawa, H. Iguchi, T. Minami *et al.*, Plasma Phys. and Control. Fusion **42**, A103 (2000).
- [16] A. Fujisawa, H. Iguchi, H. Idei *et al.*, Phys. Rev. Lett. **81**, 2256 (1998).
- [17] A. Fujisawa, H. Iguchi, T. Minami *et al.*, Phys. Rev. Lett. **82**, 2669 (1999).
- [18] A. Fujisawa, H. Iguchi, S. Lee and Y. Hamada, Rev. Sci. Instrum. **68**, 3393 (1997).
- [19] M. Kick, H. Maassberg, M. Anton *et al.*, Plasma Phys. Control. Fusion **41**, A549 (1999).
- [20] C. Alejaldre, J. Alonso, L. Almoguera *et al.*, IAEA Fusion Energy Conference 2000, Sorrento.
- [21] S. Toda and K. Itoh, *in this conference*, PII-25.
- [22] K. Itoh *et al.*, *in this conference*, PII-20.
- [23] A. Fujisawa, H. Iguchi, H. Sanuki *et al.*, Phys. Rev. Lett. **79**, 1054 (1997).
- [24] K.W. Gentle, W.L. Rowan, R.V. Bravenec *et al.*, Phys. Rev. Lett. **74**, 3620 (1995).
- [25] J.G. Cordey, D.G. Muir, V.V. Parail *et al.*, Nucl. Fusion **35**, 505(1995).
- [26] K. Itoh, S.-I. Itoh and A. Fukuyama, *Transport and Structural Formation in Plasmas*, edited by P. Scott and H. Wilhelmsson, (Institute of Phys. Pub., Bristol and Philadelphia, 1999).